Atom-molecule collisions, spin relaxation, and sympathetic cooling in an ultracold spin-polarized Rb(^2S)-SrF($^2\Sigma^+$) mixture

Masato Morita,[1] Maciej B. Kosicki,[2] Piotr S. Żuchowski,[2] and Timur V. Tscherbul[1]

[1]*Department of Physics, University of Nevada, Reno, Nevada 89557, USA*

[2]*Institute of Physics, Faculty of Physics, Astronomy and Informatics, Nicolaus Copernicus University, Grudziadzka 5, Torun 87-100, Poland*

We explore the suitability of ultracold collisions between spin-polarized SrF($^2\Sigma^+$) molecules and Rb(^2S) atoms as elementary steps for the sympathetic cooling of SrF($^2\Sigma^+$) molecules in a magnetic trap. To this end, we carry out quantum-mechanical scattering calculations on ultracold Rb + SrF collisions in a magnetic field based on an accurate potential-energy surface for the triplet electronic state of Rb-SrF developed *ab initio* using a spin-restricted coupled cluster method with single, double, and noniterative triple excitations [RCCSD(T)]. The Rb-SrF interaction has a global minimum with a well depth of 3444 cm^{-1} in a bent geometry and a shallow local minimum in the linear geometry. Despite such a strong and anisotropic interaction, we find that converged close-coupling scattering calculations on Rb + SrF collisions in a magnetic field are still possible using rotational basis sets including up to 125 closed rotational channels in the total angular momentum representation. Our calculations show that electronic spin relaxation in fully spin-polarized Rb-SrF collisions occurs much more slowly than elastic scattering over a wide range of magnetic fields (1–1000 G) and collision energies (10^{-5}–10^{-3} K), suggesting good prospects of sympathetic cooling into the microkelvin regime of laser-cooled SrF($^2\Sigma^+$) molecules with spin-polarized Rb(^2S) atoms in a magnetic trap. We show that incoming p-wave scattering plays a significant role in ultracold collisions due to the large reduced mass of the Rb-SrF collision pair. The calculated magnetic-field dependence of the inelastic cross sections at 1.4 μK displays a rich resonance structure including a low-field p-wave resonance, which suggests that external magnetic fields can be used to enhance the efficiency of sympathetic cooling in heavy atom-molecule mixtures.

I. INTRODUCTION

The production, trapping, and manipulation of cold molecular gases is expected to make a major impact on chemical physics, quantum information processing, quantum simulation, and fundamental tests of physics beyond the standard model [1]. The ability to manipulate cold molecules with external electromagnetic fields is key to the wide range of their proposed applications [2]. External field-induced Stark and Zeeman energy shifts, while insignificant at thermal collision energies, become of major importance at ultralow temperatures, where they can be used to activate or suppress reaction mechanisms [1,3–6]. A variety of ingenious mechanisms to control the reaction rates have been demonstrated experimentally, including the use of Fermi statistics, long-range dipole-dipole interactions, and external confinement to control the reaction KRb + KRb → K$_2$ + Rb$_2$ [7–9]. Recent theoretical work has explored the important roles of geometric-phase effects [10], quantum chaos [11,12], and electric-field-induced reactive scattering resonances [13] in ultracold chemical reactions.

Since its first experimental demonstration in 1998 [14], magnetic trapping remains a key experimental technique for the production and trapping of cold molecular gases. Examples of molecular radicals trapped using this technique include CaH [14], NH [15], OH [3,16], O$_2$ [17], and, more recently, CaF [18] and CH$_3$ [19]. Latest experimental advances in laser cooling [20–25] and molecular-beam deceleration have enabled magnetic and magneto-optical trapping of molecular ensembles at much lower temperatures than was previously possible. Laser-cooled samples of SrF($^2\Sigma^+$) and CaF($^2\Sigma^+$) molecules have been trapped at temperatures ⩽400 μK [21–23,25]. Additionally, efficient transfer of CaF [26] and SrF [27] molecules into a conservative quadrupole magnetic trap has recently been reported, achieving temperatures around 100 and 200 μK. More recently, sub-Doppler cooling of CaF molecules to a temperature of 60 μK has been demonstrated [28]. While experimentally demonstrated samples have low enough densities to avoid molecule-molecule collisions [26,27], they represent an ideal starting point for performing sympathetic cooling with a cotrapped atomic sample.

While extremely low compared to ambient or even cryogenic conditions ($T = 1$–4 K), millikelvin temperatures are still too high for manipulating molecular interactions with external electromagnetic fields. The primary tool for such manipulation—the magnetic Feshbach resonance [29]—requires collisions in a single partial-wave (s-wave) regime, which occur at temperatures well below 1 mK for most molecules. Direct laser-cooling and molecular-beam deceleration cannot reach such low temperatures due to their intrinsic limitations (such as the Doppler limit [23]), so alternative cooling methods must be employed to reach the ultracold regime [25].

Sympathetic cooling is one such method, based on cooling atomic and molecular species by immersion in a gas of coolant

atoms [30]. The method relies on elastic collisions to transfer momentum between the hot molecules and the coolant atoms and has been successfully used to cool fermionic K atoms [31], leading to the production of a quantum degenerate Fermi gas [32]. Inelastic collisions are detrimental to the cooling process as they release the internal (e.g., Zeeman) energy of trapped molecules, leading to undesirable heating and trap loss [1]. Spin-relaxation (or depolarization) collisions, which flip the electron spin of the molecule, represent a major inelastic channel for molecular radicals confined in permanent magnetic traps [33–35]. For optimal cooling, the ratio of the cross sections for elastic to spin-relaxation collisions γ should exceed 100 [1,36].

The search for atom-molecule combinations with favorable collisional properties for sympathetic cooling experiments has stimulated the development of molecular collision theory in the presence of magnetic fields by Volpi and Bohn [37] and Krems and Dalgarno [33]. These pioneering theoretical studies focused on collisions with He atoms and found that due to the low anisotropy of the molecule-He interaction, collision-induced spin relaxation of light $^2\Sigma$ and $^3\Sigma$ molecules with large rotational constants occurs much more slowly than elastic scattering, leading to the prediction that NH($^3\Sigma^-$) radicals could be magnetically trapped in cryogenic He buffer gas, which was later realized experimentally [15,38].

Ultracold paramagnetic atoms (such as the alkali-metal atoms or atomic nitrogen) offer a viable alternative to cryogenic helium, which is unsuitable for sympathetic cooling of molecules below 100 mK due to its vanishing vapor pressure. Ultracold alkali-metal atoms (e.g., Li, Na, Rb, and Cs) at high phase-space densities are routinely produced by laser cooling and trapping followed by evaporative cooling [39–41]. However, theoretical studies found large inelastic relaxation rates in collisions of molecular radicals OH($^2\Pi$) and NH($^3\Sigma$) with ultracold Rb atoms, suggesting that the alkali-metal atoms would be much less suitable for sympathetic cooling of magnetically trapped molecules than the alkaline-earth atoms such as Mg [42] or atomic nitrogen [43,44] or hydrogen [45], which present significant experimental difficulties associated with either trapping or detection.

More recent quantum scattering studies have shown, however, that $^2\Sigma$ molecular radicals such as CaH and SrOH have low spin-relaxation rates in collisions with ground-electronic-state Li(^2S) atoms in their maximally spin-stretched Zeeman states, despite the triplet Li-CaH and Li-SrOH interactions being extremely strong and anisotropic [46,47]. The suppression of spin relaxation is due to the weak spin-rotation coupling among the molecular rotational levels involved in spin-flipping transitions [46,48] and opens up the possibility of sympathetic cooling of $^2\Sigma^+$ molecules by ultracold Li atoms [46,47].

While atomic Li appears as a promising coolant for $^2\Sigma$ molecules, quantum scattering calculations on Li-molecule collisions performed thus far neglected the chemical reaction between cotrapped molecules and Li atoms (e.g., Li + CaH → LiH + Ca), which are energetically allowed for many $^2\Sigma^+$ molecules of interest such as CaH [46,49], SrOH [47], and SrF [50], as is the chemical reaction SrF + SrF → SrF$_2$ + Sr [51]. These reactions are often assumed to be forbidden for spin-polarized reactants by conservation of the total

spin S of the reaction complex [6,52,53]. However, model calculations show that S-changing intersystem crossing can occur at substantial rates even in fully spin-polarized atom-molecule collisions [54], triggering rapid chemical reactions [49], which are detrimental for sympathetic cooling.

Fortunately, the chemical reactions of $^2\Sigma$ molecular radicals with heavier alkali-metal atoms, such as Rb + SrF → RbF + Sr are strongly endothermic [50] and will therefore not occur at ultralow temperatures. This consideration, together with recent numerical simulations of sympathetic cooling dynamics of trapped CaF molecules [36], suggests that Rb might be a better coolant atom than Li. However, the collisional properties of $^2\Sigma$ molecular radicals with alkali-metal atoms heavier than Li remain unexplored due to the large densities of rovibrational states and strongly anisotropic atom-molecule interactions [46,47,50,55], which have thus far precluded converged quantum scattering computations on these heavy systems. As a result, it remains unclear whether the ratio of elastic to inelastic collision rates in Rb-molecule collisions is large enough to allow for efficient sympathetic cooling.

In this work, we investigate ultracold collisions in a chemically nonreactive atom-molecule mixture Rb-SrF using coupled-channel quantum scattering calculations based on an accurate *ab initio* potential-energy surface (PES) of triplet symmetry. This system can be realized experimentally by cotrapping laser-cooled SrF($X^2\Sigma$) molecules [21,23] with Rb atoms. We explore the experimentally demonstrated regime for magnetically trapped SrF samples around 200 μK and 100 G [27] providing a path to μK SrF molecules. We also show that despite a high density of rovibrational states of the Rb-SrF collision complex, it is possible to carry out converged coupled-channel (CC) calculations of elastic and inelastic cross sections using a recently developed total angular momentum representation for molecular collisions in magnetic fields [35]. We find that the ratios of elastic to inelastic cross sections, while not as favorable as for Li collisions [46,47], are nevertheless fairly large ($\gamma > 10$) over most of the collision energy and magnetic-field ranges studied, with $\gamma > 100$ reachable by tuning the external magnetic field and/or collision energy. We also find a rich resonance structure in the spin-relaxation cross sections as a function of applied magnetic field at ultralow collision energies (1.4 μK). Most of the resonance structure arises due to the incoming p partial-wave contributions, which are present even at very low collision energies due to the large reduced mass of the Rb-SrF collision complex, leading to an enhancement of the inelastic cross section. Our results suggest that the efficiency of sympathetic cooling in spin-polarized Rb-SrF($X^2\Sigma$) mixtures can be enhanced by tuning the spin-relaxation cross sections away from resonance with an applied magnetic field.

This article is organized as follows. Section II A presents our *ab initio* calculations of the triplet Rb-SrF potential-energy surface (PES) and explores the main features of the PES. Section II B outlines the methodology of our quantum scattering calculations in a magnetic field using the total angular momentum representation. Section III presents the results for the elastic and inelastic cross sections as a function of collision energy and magnetic field, along with an analysis of spin-relaxation mechanisms. Section IV concludes with a

summary of the main results and an outline of future research directions.

II. THEORY

A. *Ab initio* calculations of the triplet Rb-SrF PES

As mentioned in the Introduction, the endothermicity of the chemical reaction Rb + SrF → RbF + Sr [50] makes atomic Rb particularly attractive as a collision partner for sympathetic cooling of SrF. To pave the way for quantum dynamics calculations, we have carried out high-level *ab initio* calculations on the $^3A'$ electronic state of Rb-SrF using the state-of-the-art coupled cluster method with single, double, and noniterative triple excitations [CCSD(T)] [56,57] implemented in the MOL-PRO package [58]. The augmented core-valence, correlation-consistent basis set (aug-cc-pCVQZ) was employed to describe the F atom. For the Rb and Sr atoms, small-core relativistic energy-consistent pseudopotentials (ECP28MDF) were used together with a tailored valence basis set *spdfg*. All basis functions were uncontracted [59,60] and subsequently augmented by adding a single set of even-tempered functions. The interaction energy from the supermolecular calculations was counterpoise corrected to eliminate the basis-set super-position error (BSSE) [61]. To describe the geometry of the Rb-SrF collision complex we use the Jacobi coordinates R and θ, where R is the distance between Rb and the center of mass of SrF and θ is the angle between the SrF axis and the vector pointing from the center of mass of SrF to Rb. Throughout this paper, we assume that the SrF molecule is rigid and compute the interaction energy as a function of R and θ at a fixed SrF bond length ($r = 2.075$ Å) corresponding to the experimentally measured equilibrium geometry [62].

The *ab initio* calculations are performed on a dense two-dimensional grid of θ and R extending from 2 to 10 Å in steps of $\Delta\theta = 5°$ and $\Delta R = 0.25$ Å. For a given value of R the PES is interpolated using the reproducing kernel Hilbert space (RKHS) method [63]. The RKHS parameters were set to extrapolate the interaction energy as $-C_6 R^{-6} - C_7 R^{-7} - C_8 R^{-8}$ beyond 10 Å [30]. We monitored the stability of the coupled-cluster calculations using the T1 diagnostics [64] with a result below 0.02 for all the R grid points investigated.

The interpolated *ab initio* PES is expanded in Legendre polynomials as

$$V_\lambda(R) = \frac{1}{2}(2\lambda + 1)\int_{-1}^{1} V(R,\theta)P_\lambda(\cos(\theta))d\cos\theta. \quad (1)$$

Following Ref. [65], the angular integration is performed using the quadratures which accurately reproduce the isotropic part of the potential $V_0(R)$. Due to a very strong potential anisotropy, we used a large number of expansion terms $V_\lambda(R)$ with $\lambda \leqslant 25$. To ensure the smoothness of the potential beyond 10 Å, we used the van der Waals analytical expansion in inverse powers of R for the five leading terms ($0 \leqslant \lambda \leqslant 4$). For higher-order Legendre components the potential was damped to zero at $R > 11$ Å. A smooth connection between the *ab initio* PES at short range and the analytical expansion at long range was ensured by using the switching function introduced by Janssen *et al.* [65] between 9 and 11 Å.
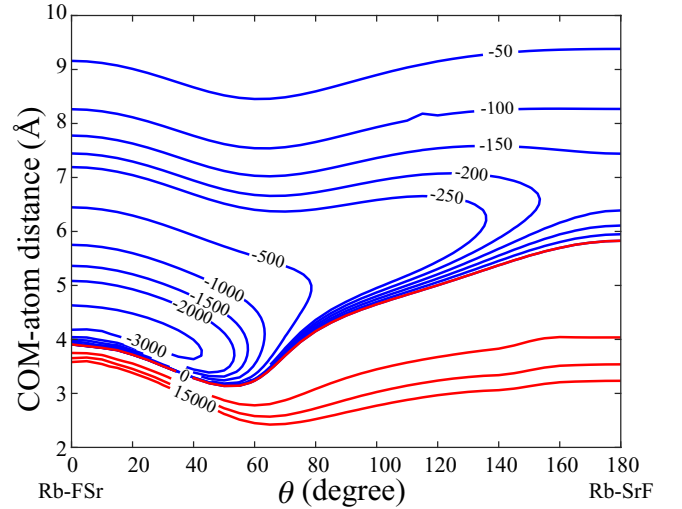

FIG. 1. Contour plot of the *ab initio* potential-energy surface for Rb-SrF in its triplet electronic state (in units of cm^{-1}). The $\theta = 0°$ geometry corresponds to the collinear Rb–F-Sr arrangement.

A contour plot of our *ab initio* PES of the Rb-SrF complex is shown in Fig. 1. The triplet PES has a global minimum in a bent configuration with $R = 4.1$ Å, $\theta = 25°$ with a well depth of $D_e = 3444$ cm^{-1}. Here and elsewhere except Sec. IIB, we express energy in units of wave numbers (cm^{-1}), which are commonly used to measure energy in spectroscopy and molecular physics [66]. By definition, the wave number $\tilde{\nu} = 1/\lambda$ is the number of wavelengths λ per 1 cm. While wave numbers are, strictly speaking, not energy units, they are directly proportional to energy via $E = hc\tilde{\nu}$, where h is Planck's constant and c is the speed of light in vacuum. As a point of reference, 1 cm$^{-1} = 4.55633 \times 10^{-6}$ atomic units of energy [66].

The Rb-SrF interaction potential is extremely anisotropic, leading one to expect strong coupling between the rotational states of SrF in the collision complex. There are two saddle points on the PES, both at linear geometries. For the Sr-F-Rb configuration the saddle point is located at $R = 4.25$ Å, while for the Rb-Sr-F configuration it is located at $R = 6.80$ Å. It is worthwhile to note that the global minimum of the triplet PES is strongly attractive even at the restricted Hartree-Fock level of theory (about 2900 cm^{-1} near the global minimum). This implies that the inaccuracy of our *ab initio* PES should be smaller than that of typical dispersion-bound systems. To estimate the inaccuracy due to the incompleteness of the basis set, we compare in Table I the interaction energies near the stationary points of the PES obtained with series of basis sets of different quality, ranging from triple to quintuple zeta, as well as with the approximate complete basis set (CBS) limit. Clearly, the depth of the potential near the global minimum and the Rb-F-Sr saddle point changes very little with increasing basis set size. Moreover, we observe that all the stationary points behave very similarly at the quintuple zeta level and in the CBS, so the shape of the PES is insensitive to the basis set. The global minimum obtained with the quadruple-zeta basis set, which was used in production calculations, is underestimated by 2.2% compared to the CBS limit. The

TABLE I. Convergence of the absolute magnitude of the interaction energy with the basis set size at the global minimum ($R = 4.1$ Å, $\theta = 25°$) and two saddle points at linear geometries: Rb-F-Sr (with $R = 4.25$ Å) and Rb-Sr-F ($R = 6.8$ Å). The energy unit is cm^{-1}.

	aug-cc-pCVTZ	aug-cc-pCVQZ	aug-cc-pCV5Z	CBS
Global minimum	3329	3444	3485	3521
Rb-F-Sr saddle point	3093	3243	3292	3337
Rb-Sr-F saddle point	170	172	173	175

corresponding figures for the Rb-Sr-F and Rb-F-Sr saddle points are 1.7% and 2.8%, respectively. Since the interaction energy of Rb-SrF is not dominated by the dispersion interaction, the contributions of higher excitations are marginal and we expect the CCSD(T) method to accurately reproduce the interaction energy.

B. Quantum scattering calculations

The quantum scattering problem for Rb + SrF in a magnetic field is solved by the numerical integration of close-coupling (CC) equations using the total angular momentum representation in the body-fixed (BF) coordinate frame [35,46]. We employ the rigid-rotor approximation by constraining the SrF bond length to the ground-state equilibrium value of $r = 2.075$ Å. The approximation is justified by recent *ab initio* calculations [50], which show that the Rb-SrF interaction depends on r only weakly.

The effective Hamiltonian for low-energy collisions between a ^2S atom A (Rb) and a $^2\Sigma$ diatomic molecule B (SrF) in the presence of an external magnetic field may be written using the atomic units ($\hbar = e = m_e = 1$) [35,46]

$$\hat{\mathcal{H}} = -\frac{1}{2\mu}R^{-1}\frac{d^2}{dR^2}R + \frac{(\hat{J} - \hat{N} - \hat{S}_A - \hat{S}_B)^2}{2\mu R^2} + \hat{\mathcal{H}}_A + \hat{\mathcal{H}}_B + \hat{\mathcal{H}}_{\text{int}}, \quad (2)$$

where A and B stand for Rb and SrF, μ is the reduced mass of the A-B collision complex $\mu = m_A m_B/(m_A + m_B)$ with $m_A = 86.909\,180\,527$ and $m_B = 106.904\,015\,32$ a.m.u, $\hat{\mathcal{H}}_A$ and $\hat{\mathcal{H}}_B$ describe noninteracting collision partners in an external magnetic field, and $\hat{\mathcal{H}}_{\text{int}}$ is the atom-molecule interaction, which vanishes in the limit $R \to \infty$. The embedding of the BF z axis is chosen to coincide with the vector $\mathbf{R}$, and the BF y axis is chosen to be perpendicular to the plane defined by the collision complex (see Appendix A for more details).

In Eq. (2), $\hat{J}$ is the operator for the total angular momentum of the collision complex, $\hat{N}$ is that for the rotational angular momentum of the diatomic molecule, and $\hat{S}_A$ and $\hat{S}_B$ are the operators for the electronic spin angular momenta of atom A and molecule B. The orbital angular momentum operator of the collision complex in the BF frame is given by $\hat{l} = (\hat{J} - \hat{N} - \hat{S}_A - \hat{S}_B)$. The Hamiltonian of atom A is given by $\hat{\mathcal{H}}_A = g_e \mu_B \hat{S}_{A,Z} B$, where g_e is the electron g factor, μ_B is the Bohr magneton, $\hat{S}_{A,Z}$ gives the projection of $\hat{S}_A$ onto the space-fixed Z axis defined by the direction of an external magnetic field $\mathbf{B}$, and $B = |\mathbf{B}|$ is the field magnitude. The Hamiltonian of the diatomic molecule B in its ground electronic state of $^2\Sigma$ symmetry (such as SrF) is

$$\hat{\mathcal{H}}_B = B_e \hat{N}^2 + \gamma_{\text{SR}} \hat{N} \cdot \hat{S}_B + g_e \mu_B \hat{S}_{B,Z} B, \quad (3)$$

where $B_e = 0.253\,613\,5$ cm^{-1} is the rotational constant and $\gamma_{\text{SR}} = 2.501 \times 10^{-3}$ cm^{-1} is the spin-rotation constant (the values for the ^{88}Sr^{19}F isotope from Ref. [22]). In this work, we neglect the weak hyperfine interactions due to the nuclear spins of ^{87}Rb and ^{88}Sr^{19}F for the sake of computational efficiency [adding these interactions would increase the number of channels by a factor of $(2I_A + 1) \times (2I_B + 1) = 8$, increasing the computational cost over 100-fold]. In the regime where the Zeeman splitting is small compared to the hyperfine interaction, scattering calculations omitting the latter are known to underestimate the actual values of spin-relaxation cross sections [67]. The critical value of the magnetic field above which the hyperfine interactions become small compared to the Zeeman interaction (and hence can be neglected) is given by $B_c = \Delta_{10}/\mu_B = 77$ G, where $\Delta_{10} = 107.9$ MHz is the ground-state hyperfine splitting of ^{88}Sr^{19}F ($I_B = 1/2$) calculated using the molecular constants from Ref. [22]. Thus our results at $B \geqslant 100$ G are likely to be only weakly affected by the hyperfine interaction.

The atom-molecule interaction given by the $\hat{\mathcal{H}}_{\text{int}}$ term in Eq. (2) includes both the electrostatic interaction potential $\hat{V}$ and the magnetic dipole-dipole interaction $\hat{V}_{\text{dd}}$ between the magnetic moments of A and B. The interaction potential $\hat{V}$ may be written

$$\hat{V}(R,\theta) = \sum_{S=|S_A - S_B|}^{S_A + S_B} \sum_{\Sigma=-S}^{S} |S\Sigma\rangle \hat{V}^S(R,\theta)\langle S\Sigma|, \quad (4)$$

where total electronic spin S is defined as $\hat{S} = \hat{S}_A + \hat{S}_B$. In this work, we are interested in collisions between rotationally ground-state SrF molecules ($N = 0$) with Rb atoms initially in their maximally stretched, magnetically trappable Zeeman states, i.e., $M_{S_A} = M_{S_B} = 1/2$, where M_{S_A} and M_{S_B} are the projections of $\hat{S}_A$ and $\hat{S}_B$ onto the magnetic-field axis. Following our previous work on Li-CaH and Li-SrOH [46,47] we assume that the nonadiabatic coupling between the triplet ($S = 1$) and the singlet ($S = 0$) Rb-SrF PESs can be neglected, and that the PESs are identical, i.e., $\hat{V}^{S=0}(R,\theta) = \hat{V}^{S=1}(R,\theta)$. The magnetic dipole-dipole interaction may be written [68]

$$\hat{V}_{\text{dd}} = -g_e^2 \mu_0^2 \sqrt{\frac{24\pi}{5}} \frac{\alpha^2}{R^3} \sum_q (-1)^q Y_{2,-q}^*(\hat{\mathbf{R}})[\hat{S}_A \otimes \hat{S}_B]_q^{(2)}, \quad (5)$$

where μ_0 is the magnetic permeability of free space, α is the fine-structure constant, and $[\hat{S}_A \otimes \hat{S}_B]_q^{(2)}$ is the spherical tensor product of $\hat{S}_A$ and $\hat{S}_B$.

Following previous theoretical work [35,46,68], the total wave function of the Rb-SrF collision complex is expanded in a set of basis functions

$$|JM\Omega\rangle|NK_N\rangle|S_A\Sigma_A\rangle|S_B\Sigma_B\rangle, \quad (6)$$

where Ω, K_N, Σ_A, and Σ_B are the projections of J, N, S_A, and S_B onto the standard BF axis z' (see Appendix A) and $\Omega = K_N + \Sigma_A + \Sigma_B$. The basis functions in Eq. (6) are direct products of four state vectors. The first state vector describes the rotation of the rigid atom-molecule collision complex in three dimensions, and may be written as $|JM\Omega\rangle = (\frac{2J+1}{4\pi})^{1/2} D^{J*}_{M\Omega}(\bar{\alpha}, \bar{\beta}, \bar{\gamma})$, where $\bar{\alpha}$, $\bar{\beta}$, and $\bar{\gamma}$ are the Euler angles that specify the orientation of the standard body-fixed (BF) frame relative to the SF frame and $D^J_{M\Omega}(\bar{\alpha}, \bar{\beta}, \bar{\gamma})$ is a Wigner D function [69]. As shown in Appendix A (see also Refs. [70,71]) the third Euler angle $\bar{\gamma} = \phi$, where ϕ is the azimuthal angle of the diatomic molecule in the two-thirds BF frame shown in Fig. 5(a). The second state vector $|NK_N\rangle = Y_{NK_N}(\theta, 0)$ belongs to the Hilbert space of a rigid rotor (the diatomic molecule B), where the polar angle θ is the polar angle of the molecular axis in the standard BF frame (see Appendix A). The state vectors $|S_A\Sigma_A\rangle$ and $|S_B\Sigma_B\rangle$ are in the Hilbert space of a spin-S_A (or spin-S_B) system, which accounts for the spin degrees of freedom of atom A (or molecule B). Note that the projections Σ_A and Σ_B are defined with respect to the BF z-axis $\mathbf{R}$.

The BF basis (6) is closely related to the standard SF total angular momentum basis of eigenfunctions of $\hat{J}^2$ and $\hat{J}_Z$ widely used in molecular collision theory [72]. Here, Z stands for the SF Z axis defined by the direction of an external magnetic field. The SF basis functions can be obtained by vector coupling of all angular momenta in the system

$$|JM(lJ_{AB}J_B S_A S_B N)\rangle = \sum_{M_{AB}, m_l} \langle J_{AB} M_{AB} l m_l | JM \rangle$$
$$\times |J_{AB}M_{AB}(J_B S_A S_B N)\rangle |lm_l\rangle, \quad (7)$$

where $\langle \cdots | \cdot\cdot \rangle$ are the Clebsch-Gordan coefficients, $\hat{J} = \hat{l} + \hat{S}_A + \hat{S}_B + \hat{N}$ is the total angular momentum of the collision complex, $\hat{J}_{AB} = \hat{S}_A + \hat{J}_B$ is the combined angular momentum of atom A and diatomic molecule B, $\hat{J}_B = \hat{S}_B + \hat{N}$ is the total angular momentum of the diatomic molecule, and $|lm_l\rangle$ are the eigenstates of $\hat{l}^2$ and $\hat{l}_Z$. The functions $|J_{AB}M_{AB}(J_B S_A S_B N)\rangle$ on the right-hand side of Eq. (7) are obtained by vector coupling of the eigenstates of $\hat{J}_B^2$ and $\hat{J}_{B_Z}$ and those of $\hat{S}_A^2$ and $\hat{S}_{A_Z}$.

We further note that the quantum number J of the BF state $|JM\Omega\rangle$ is the same as that of the SF state $|JM(lJ_{AB}J_B S_A S_B N)\rangle$ in Eq. (7) because these states are

related by an orthogonal rotation transformation $\hat{\mathcal{R}}(\bar{\alpha}, \bar{\beta}, \bar{\gamma})$, which transforms the SF axes to the BF axes [69]. Because the rotation operator $\hat{\mathcal{R}}(\bar{\alpha}, \bar{\beta}, \bar{\gamma})$ commutes with the total angular momentum operator of the system J^2, the value of J is unchanged by the rotation transformation as discussed in more detail in Sec. 3.5 of Ref. [69] [see also Eq. (17) of Tennyson and Sutcliffe [73]].

The BF and SF states given by Eqs. (6) and (7) are related by an orthogonal transformation

$$|JM(lJ_{AB}J_B S_A S_B N)\rangle$$
$$= \sum_{\alpha, \Omega} W^{JM}_{\Omega N K_N S_A \Sigma_A S_B \Sigma_B; lJ_{AB}J_B S_A S_B N}$$
$$\times |JM\Omega\rangle |NK_N\rangle |S_A\Sigma_A\rangle |S_B\Sigma_B\rangle, \quad (8)$$

where the coefficients $W^{JM}_{\Omega N K_N S_A \Sigma_A S_B \Sigma_B; lJ_{AB}J_B S_A S_B N}$ form an orthogonal matrix $\mathbf{W}$, which can be obtained by diagonalizing the matrix of $\hat{l}^2 = (\hat{J} - \hat{N} - \hat{S}_A - \hat{S}_B)^2$ in the BF basis (6) as described in our previous work [35]. The transformation (8) does not mix basis functions with different values of J, M, and N [35]. An advantage of the SF total angular momentum basis (7), (8) is that it provides a representation that diagonalizes the operator $\hat{l}^2 = (\hat{J} - \hat{N} - \hat{S}_A - \hat{S}_B)^2$ in Eq. (2) and thus each SF basis function has a definite value of l as required for the application of scattering boundary conditions. We transform the log-derivative matrix to the SF basis after reaching the outer end of the integration grid (see below and Ref. [35]).

Scattering calculations in external fields can also be carried out using the fully uncoupled SF basis [33,37]. While these calculations provide an independent test of the results computed here using the BF basis (see Appendix B) the SF basis sets become too computationally expensive already for $N_{max} \geqslant 7$, and thus cannot be used to obtain converged results for strongly anisotropic Rb + SrF collisions [34,46].

In the presence of an external magnetic field, the projection M of the total angular momentum J onto the magnetic-field axis M is conserved (unlike J itself) [33,35] and we solve the CC equations separately for each value of M. The matrix elements of the effective Hamiltonian in the total angular momentum representation (6) are evaluated as described elsewhere [35]. The matrix elements of the magnetic dipole-dipole interaction $\hat{V}_{dd}$ are

$$\langle J'M\Omega' | \langle N'K'_N | \langle S_A\Sigma'_A | \langle S_B\Sigma'_B | \hat{V}_{dd} | S_B\Sigma_B\rangle | S_A\Sigma_A\rangle | NK_N\rangle | JM\Omega\rangle$$

$$= \delta_{J'J}\delta_{\Omega'\Omega}\delta_{N'N}\delta_{K'_N, K_N} \left(-\frac{\sqrt{30}g_e^2\mu_0^2\alpha^2}{R^3} \right) (-1)^{S_A + S_B - \Sigma_A - \Sigma_B} \sqrt{(2S_A + 1)S_A(S_A + 1)} \sqrt{(2S_B + 1)S_B(S_B + 1)}$$

$$\times \sum_{q_A, q_B} \begin{pmatrix} 1 & 1 & 2 \\ q_A & q_B & 0 \end{pmatrix} \begin{pmatrix} S_A & 1 & S_A \\ -\Sigma'_A & q_A & \Sigma_A \end{pmatrix} \begin{pmatrix} S_B & 1 & S_B \\ -\Sigma'_B & q_B & \Sigma_B \end{pmatrix}. \quad (9)$$

The size of the basis set is determined by the truncation parameters of J_{max} and N_{max} which give the maximum quantum numbers of the total angular momentum J of the collision complex and the rotational angular momentum N of SrF in the basis set. We use the values $J_{max} = 3$ and $N_{max} = 125$

that give the elastic and inelastic cross sections converged to $\leqslant 2.5\%$ (see Appendix C). The numerical procedures used in this work are essentially the same as those employed in our previous studies of Li + CaH and Li + SrOH collisions [46,47]. The CC equations are solved numerically using the

log-derivative propagator method [74,75] on an equidistant radial grid from $R_{\min} = 5.2$ Bohr to R_{mid} with $R_{\mathrm{mid}} = 15.0$ Bohr for $B \geqslant 10$ G and $R_{\mathrm{mid}} = 25.0$ Bohr for $B < 10$ G using a step size of 0.002 Bohr. Airy propagation is employed for $R_{\mathrm{mid}} \leqslant R \leqslant R_{\max}$ with $R_{\max} = 300.0$ Bohr for $B \geqslant 10$ G and $R_{\max} = 750$ Bohr for $B < 10$ G. At $R = R_{\max}$, we transform the log-derivative matrix from the BF total angular momentum representation (6) to the SF basis (7) via Eq. (8). In spite of providing a diagonal representation for the operator l^2, the asymptotic Hamiltonian $\hat{\mathcal{H}}_A + \hat{\mathcal{H}}_B$ [the $R \to \infty$ limit of Eq. (2)] is not diagonal in either BF or SF representations due to the presence of an external magnetic field, which couples basis functions of different J, so an additional change of basis is required to bring the asymptotic Hamiltonian to a diagonal form [35]. The matrix of this final transformation is composed of the eigenvectors of the asymptotic Hamiltonian in the SF basis (7). After all of these transformations, the log-derivative matrix is matched to the scattering boundary conditions to obtain the S-matrix following standard numerical techniques [76]. The scattering cross sections are computed from the S-matrix elements as described in, e.g., Refs. [35,68].

III. RESULTS

A. Elastic and inelastic cross sections

Figure 2(a) shows the elastic and inelastic cross sections for spin-polarized Rb + SrF collisions plotted as functions of collision energy for the external magnetic fields of 1, 100, and 1000 G. The internal state of SrF($X^2\Sigma^+$) before the collision is $|N = 0, M_N = 0, M_{S_B} = 1/2\rangle$ and that of Rb(^2S) is $|M_{S_A} = 1/2\rangle$. At very low collision energies of interest here (which are much smaller than the rotational energy splitting between the ground $N = 0$ and the first excited, $N = 1$ rotational states of SrF), the only inelastic process that can occur is electronic spin relaxation within the ground rotational state, i.e., $|N = 0, M_N = 0, M_{S_B} = 1/2\rangle \to |N' = 0, M'_N = 0, M'_{S_B} = -1/2\rangle$. The field dependence of the elastic cross section is very weak, and thus only the $B = 1000$ G result is shown in Fig. 2(a). We observe that the inelastic cross section decreases with increasing the magnetic field from 1 G to 1000 G; the effect is particularly strong in the ultracold s-wave regime.

A key figure of merit for sympathetic cooling is the ratio of elastic to inelastic cross sections $\gamma = \sigma_{\mathrm{el}}/\sigma_{\mathrm{inel}}$; $\gamma > 100$ is generally required for optimal sympathetic cooling of magnetically trapped molecules [1,36,46,47]. Figure 2(b) shows that the calculated values of γ for Rb + SrF collisions exceed 100 at collision energies above $E_C \sim 5 \times 10^{-5}$ cm^{-1}, suggesting good prospects for sympathetic cooling of cold SrF($^2\Sigma^+$) molecules with magnetically cotrapped Rb atoms. At ultralow collision energies ($E_C < 10^{-5}$ cm^{-1}) the ratio of elastic to inelastic collision rates drops below 100 and becomes very sensitive to the applied magnetic field. Still, we observe that the inelastic cross sections are relatively small at $B = 1000$ G compared with their values at smaller magnetic fields. Thus, as noted previously for He + O$_2$ [77] and Li + SrOH [47], it may be possible to enhance the efficiency of sympathetic cooling by tuning the inelastic cross sections with an applied magnetic field.
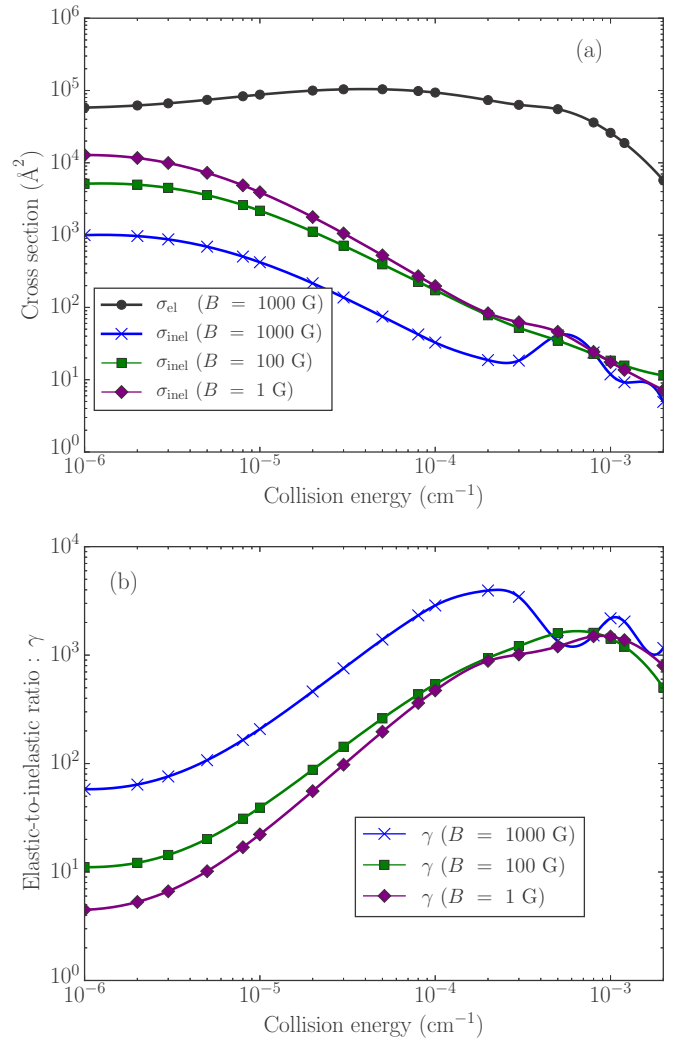

FIG. 2. (a) Collision energy dependence of the elastic cross section (circles) and inelastic cross section for the external magnetic field of 1 G (diamonds), 100 G (squares), and 1000 G (crosses). The elastic cross section displays a very weak field dependence. (b) The ratios of elastic and inelastic cross sections as functions of collision energy for the same values of the magnetic field as in (a).

Figures 3(a) and 3(b) show incoming partial-wave contributions to the elastic and inelastic cross sections at $B = 100$ G. Based on the *ab initio* value of the long-range dispersion coefficient $C_6 = 3495$ a.u. [50], the calculated heights of the p- and d-wave centrifugal barriers are 5.53×10^{-5} and 2.87×10^{-4} cm^{-1}. Consistent with these estimates, we observe in Fig. 3(a) a decline of $l \geqslant 1$ incoming partial-wave contributions to the elastic cross section as the collision energy is tuned below the corresponding barrier heights.

Remarkably, the p-wave contribution to the *inelastic* cross section dominates through the entire collision energy range spanning three orders of magnitude ($E_C = 10^{-6}$–2×10^{-3} cm^{-1}). This suggests the presence of a near-threshold scattering resonance, as discussed in more detail below. In contrast, the partial-wave spectrum of the inelastic cross sections calculated previously for Li + CaH and Li + SrOH [47] is dominated by the incoming s-wave contributions below
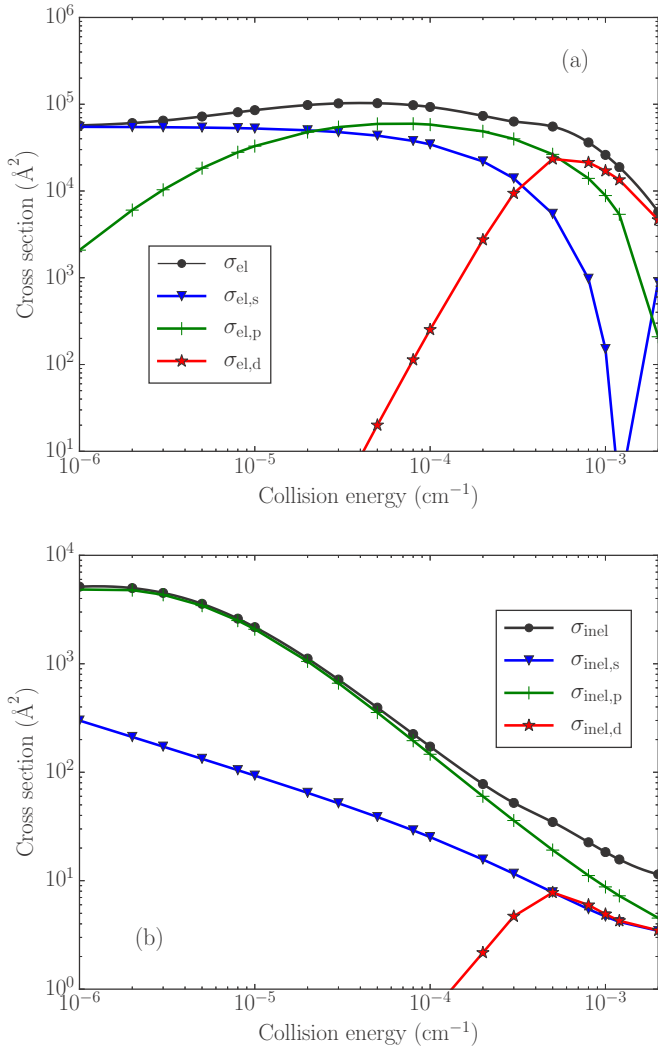
FIG. 3. Incoming partial-wave decomposition of the elastic (a) and inelastic (b) cross sections as a function of collision energy calculated for the magnetic field of 100 G. The total elastic and inelastic cross sections are shown as solid lines with circles.

$E_C = 10^{-3}$ cm^{-1} and by all partial waves at higher collision energies.

B. Magnetic-field dependence and spin-relaxation mechanisms

In Fig. 4(a), we plot the magnetic-field dependence of the cross sections for elastic scattering and spin relaxation in spin-polarized Rb-SrF collisions at a collision energy of 10^{-6} cm^{-1}. We observe a broad resonance profile in the inelastic cross section centered at $B = 0.2$ G, where inelastic scattering occurs 2.6 times faster than elastic scattering. With further increase in magnetic field, the inelastic cross section decreases by more than an order of magnitude, whereas the elastic cross section remains essentially independent of the field. A dense resonance pattern emerges above $B = 100$ G, where the ratio of elastic to inelastic cross sections γ varies rapidly from unity to above 100. Thus it may be possible to enhance the efficiency of sympathetic cooling by tuning the inelastic cross sections with an applied magnetic field.
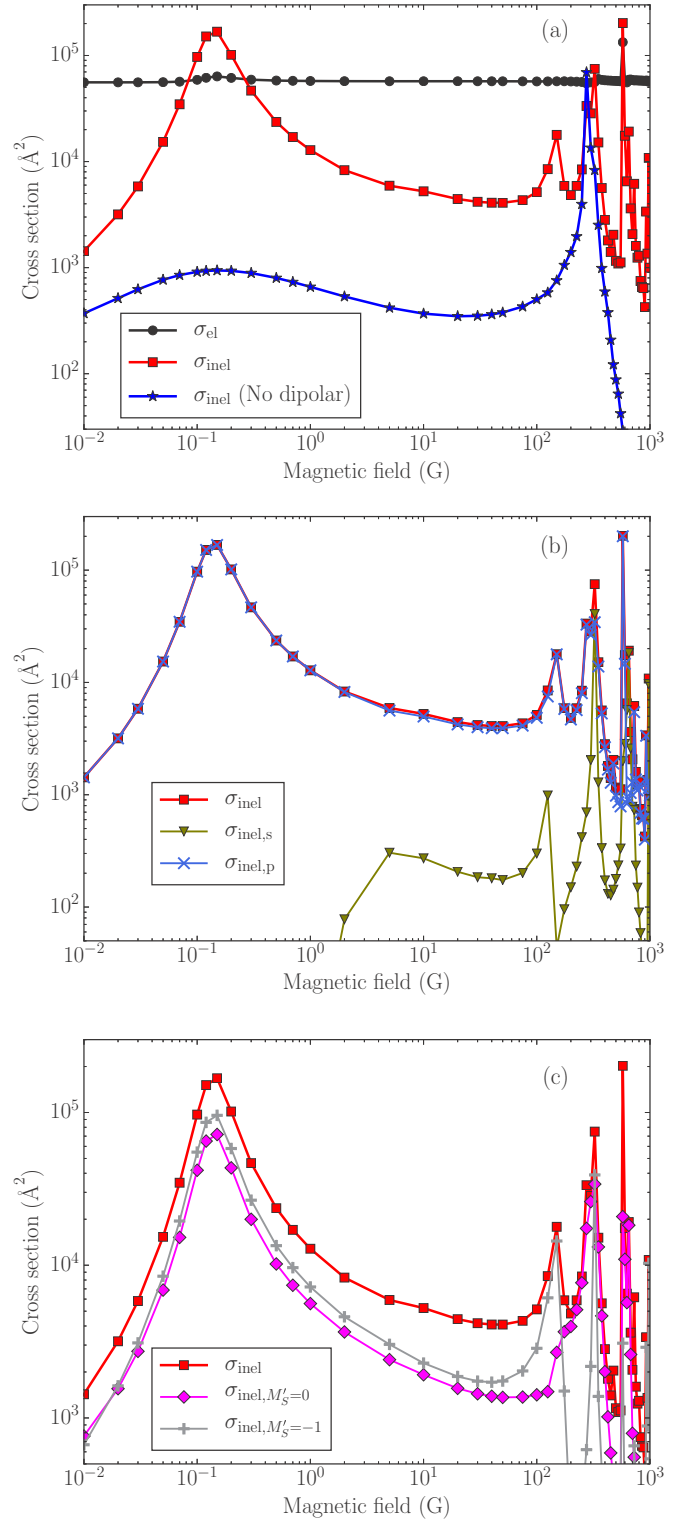

FIG. 4. (a) Magnetic-field dependence of the elastic (circles) and inelastic (squares) cross sections calculated for the collision energy of 10^{-6} cm^{-1}. The inelastic cross sections calculated with the magnetic dipole-dipole interaction omitted are shown as stars. (b) Incoming partial-wave decomposition of the inelastic cross section. (b) Final-state decomposition of the inelastic cross section.

Spin relaxation in ultracold collisions of $^2\Sigma$ molecules in their ground rotational states with ^2S atoms is mediated by two mechanisms, direct and indirect [46,48]. The direct

mechanism is due to the long-range magnetic dipole-dipole interaction between the electronic spins of the collision partners given by the term $\hat{V}_{dd}$ in Eq. (5) [46,47,78,79]. The indirect mechanism is a combined effect of the intramolecular spin-rotation interaction and the coupling between the rotational states of the molecule induced by the anisotropy of the interaction potential [46,48]. Previous theoretical studies have found that spin-relaxation in Li + CaH and Li + SrOH collisions occur predominantly via a direct mechanism and that the indirect mechanism is strongly suppressed at low collision energies ($E_C < 10^{-3}$ cm^{-1}) [46,47]. In order to compare these mechanisms for Rb + SrF collisions, we plot in Fig. 4(a) the inelastic cross section calculated with the magnetic dipole-dipole interaction term $\hat{V}_{dd}$ omitted from the scattering Hamiltonian. We observe a dramatic reduction of the spin-relaxation cross section over the entire magnetic-field range, except for a narrow resonance at $B = 250$ G.

In order to further inspect the spin-relaxation mechanisms, we show in Fig. 4(b) the incoming partial-wave contributions to the inelastic cross section. Below $B = 300$ G, the inelastic cross section is dominated by the incoming p-wave contribution. The incoming s-wave contribution becomes comparable in magnitude in the vicinity of scattering resonances. The results plotted in Figs. 4(a) and 4(b) allow us to conclude that spin relaxation in spin-polarized Rb + SrF collisions is driven by the magnetic dipole-dipole interaction between the electron spins of Rb and SrF.

As follows from Eq. (5), the magnetic dipole-dipole interaction has nonzero matrix elements between all of the $|M_{S_A}\rangle|M_{S_B}\rangle$ spin basis states. This long-range interaction can thus cause either single spin-flip relaxation, in which the electron spins of either Rb or SrF are flipped, or double spin-flip relaxation, in which both of the electron spins are flipped. The projection of the total electron spin of the Rb-SrF complex on the magnetic-field axis $M_S = M_{S_A} + M_{S_B}$ changes by 1 in a single spin-flip transition ($|M_S = 1\rangle \rightarrow |M_S' = 0\rangle$) and by 2 in a double spin-flip transition ($|M_S = 1\rangle \rightarrow |M_S' = -1\rangle$). In contrast, the indirect mechanism mediated by the spin-rotation interaction [48] can only change the projection of the molecule's electron spin M_{S_B}, and thus only the single-flip $M_S = 1 \rightarrow M_S' = 0$ transition is allowed.

Figure 4(c) shows the final state-resolved inelastic cross sections for Rb-SrF collisions. We observe that double spin-flip relaxation is slightly more efficient than single spin-flip relaxation at low magnetic fields. Interestingly, the double spin-flip relaxation occurs without changing the initial partial-wave component, via the process $|M_S = 1\rangle|l = 1, M_l = -1\rangle \rightarrow |M_S' = -1\rangle|l' = 1, M_l' = 1\rangle$ within the ground rotational state manifold ($N = N' = 0$). This is consistent with the p-wave resonance-mediated mechanism considered above.

IV. SUMMARY AND CONCLUSIONS

We have presented an *ab initio* study of ultracold collisions in a heavy, spin-polarized mixture of Rb(^2S) atoms and SrF($X\,^2\Sigma^+$) molecules in the presence of an external magnetic field. We developed an accurate *ab initio* interaction PES for the triplet $^3A'$ electronic state of Rb-SrF using the state-of-the-art CCSD(T) method and large correlation-consistent basis sets. The PES features a deep

minimum and an extremely steep dependence on the Rb-SrF bending angle θ (Fig. 1), making the Rb-SrF interaction strongly anisotropic. Using the *ab initio* PES, we carried out converged quantum scattering calculations using the total angular momentum representation in the BF coordinate frame [35], demonstrating the feasibility of such calculations on heavy, strongly anisotropic atom-molecule collision systems.

The inelastic collisions change the value of the molecule's electron spin projection M_S on the magnetic-field axis, leading to magnetic trap loss. The ratio γ of elastic to inelastic collision rates is a key predictor of successful atom-molecule sympathetic cooling in a magnetic trap. Our calculations show that ultracold spin-polarized Rb-SrF mixtures are relatively stable against collisional relaxation ($\gamma > 10$) over most of the collision energy and magnetic-field ranges explored in this work ($E_C = 10^{-6}$–10^{-3} cm^{-1} and $B = 0.01$–1000 G). It is important to point out, however, that small changes in the Rb-SrF PES can lead to dramatic variations of the scattering cross sections. Because the estimated uncertainty in our PES is about 5%, our scattering calculations presented in this paper should be considered as qualitatively accurate. A detailed analysis of the effect of the uncertainties of the interaction potentials will be presented in future work.

Our calculations predict a significant magnetic-field dependence of the inelastic cross section at ultralow collision energies (see Fig. 4), which suggests the possibility of tuning inelastic collision rates by applying an external magnetic field to optimize the efficiency of sympathetic cooling, as suggested before for He-O$_2$ and Li-SrOH [47,77]. The inelastic spin relaxation in cold Rb + SrF collisions is mainly driven by a direct mechanism mediated by the magnetic dipole-dipole interaction between the electronic spins of Rb and SrF.

It is instructive to compare the collisional properties of Rb + SrF with those of the lighter collision systems Li + SrOH and Li + CaH explored in our previous work [46,47]. While the potential depths and anisotropies are comparable in all of the alkali-molecule systems, the lighter reduced masses of Li-containing complexes result in higher centrifugal barriers. As a result, the s-wave regimes of Li + SrOH and Li + CaH collisions occur at higher collision energies. In addition, as mentioned in Sec. III A, the presence of a near-threshold p-wave resonance at low magnetic fields modifies the Wigner scaling of Rb-SrF spin relaxation cross sections, making them almost independent of the collision energy [see Fig. 4(b)]. In contrast, the spin-relaxation cross sections for Li + CaH and Li + SrOH collisions exhibit the expected s-wave Wigner scaling as $E_C \rightarrow 0$ with $\sigma_{\text{inel}} \propto E_C^{-1/2}$. Finally, the resonance peaks in the magnetic-field dependence of the spin-relaxation cross sections for Rb + SrF are much narrower than those calculated previously for Li + SrOH [47]. This suggests that the resonances in Rb + SrF collisions decay mainly by tunneling through a p-wave centrifugal barrier in the incoming collision channel, whereas those in Li + SrOH collisions decay by a mechanism not involving tunneling in the incoming channel.

In future work, it would be interesting to explore the collisional properties of nonfully spin-polarized initial states of Rb and SrF (which would require explicit consideration of the singlet Rb-SrF PES) and elucidate the effects of hyperfine interactions on scattering observables at low magnetic fields.

Experimental measurements of inelastic collision rates in ultracold Rb-SrF mixtures as a function of magnetic field would be desirable to constrain the interaction PES. Finally, it would be worthwhile to extend this study to other $^2\Sigma$ molecules currently under experimental investigation (such as CaF and YO [24,26]) and lighter coolant atoms (such as K).

APPENDIX A: COORDINATE FRAMES AND BASIS FUNCTIONS

Here, we define the SF and BF coordinate frames for the atom-molecule collision complex along with the corresponding basis functions. In the following we will omit the spin basis functions for the sake of simplicity, setting $\Sigma_A = \Sigma_B = 0$, and hence $\Omega = K_N$. The discussion can be easily generalized to include nonzero atomic and molecular spin functions $|S_A \Sigma_A\rangle$ and $|S_B \Sigma_B\rangle$.

We begin by defining the "two-thirds" BF frame (sometimes also called the "two-angle embedding" frame [80]). The z axis of the two-thirds BF frame coincides with the atom-molecule Jacobi vector **R** whose orientation relative to the SF axes X, Y, and Z is specified by the polar $\bar{\beta}$ and azimuthal $\bar{\alpha}$ angles as shown in Fig. 5(a). We assume that Z is defined by the direction of an external magnetic field. The angles $(\bar{\beta}, \bar{\alpha})$ are the two Euler angles that define the orientation of the z axis of the two-thirds BF frame relative to the SF axes. To completely specify the orientation of the x and y axes, we need to choose the third Euler angle $\bar{\gamma}$, which is the angle between the line of nodes (the intersection of the XY and xy planes) and the y axis [69]. Alternatively, $\bar{\gamma}$ can be thought of as the azimuthal angle about the z axis [see Fig. 5(a) and Fig. 3.1 of Ref. [69]]. We follow previous theoretical work [70,80] in choosing the third Euler angle $\bar{\gamma} = 0$, which means that the two-third BF y axis lies in the XY plane. The polar and azimuthal angles of the diatomic molecule in the two-thirds BF frame are denoted as θ and ϕ [see Fig. 5(b)]. These angles, together with the Euler angles $(\bar{\alpha}, \bar{\beta})$ defined above, constitute the four angular variables that are necessary to specify the configuration of the atom-molecule system. Note that the definition of the two-thirds BF axes does not depend on the orientation of the diatomic molecule vector **r**.

In the two-thirds BF frame, the basis function $|JM\Omega\rangle = [(2J+1)/4\pi]^{1/2} D_{M\Omega}^{J*}(\bar{\alpha}, \bar{\beta}, 0)$ in Eq. (6) is a function of two Euler angles $(\bar{\alpha}, \bar{\beta})$ defined above and shown in Fig. 5(a) [70]. The basis functions for the $\hat{\mathbf{R}} = \mathbf{R}/R$ and $\hat{\mathbf{r}} = \mathbf{r}/r$ vectors in the two-thirds BF frame can be written as [70]

$$\left(\frac{2J+1}{4\pi}\right)^{1/2} D_{M\Omega}^{J*}(\bar{\alpha}, \bar{\beta}, 0) Y_{NK_N}(\theta, \phi). \tag{A1}$$

(Note that the normalization factor $[(2J+1)/4\pi]^{1/2}$ is larger by $\sqrt{2\pi}$ than the standard factor $[(2J+1)/8\pi^2]^{1/2}$ because of the absence of integration over $\bar{\gamma}$.)
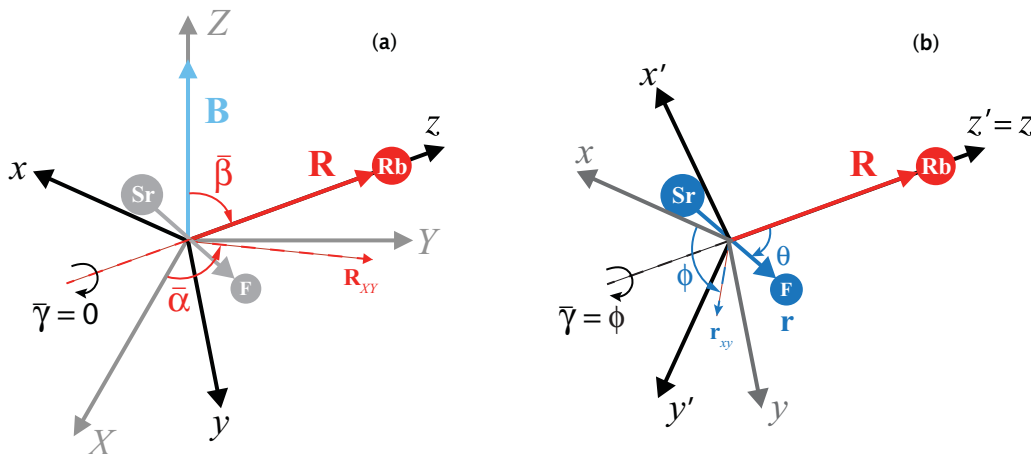

FIG. 5. Schematic depiction of the two-thirds BF frame (a) and the standard BF frame (b). The SF axes are denoted X, Y, and Z, with the Z axis defined by the direction of the applied magnetic field **B**. The orientation of the BF axes x, y, and z with respect to the SF axes is specified by the Euler angles $\bar{\alpha}$, $\bar{\beta}$, and $\bar{\gamma}$ defined according to the convention adopted in Ref. [69]. The z axis of the two-thirds BF frame coincides with the atom-molecule Jacobi vector **R** which has polar coordinates $\bar{\beta}$, $\bar{\alpha}$ in the SF frame ($\mathbf{R}_{XY}$ is the projection of **R** onto the XY plane). The third Euler angle is the angle between the line of nodes (the intersection of the XY and xy planes) and the y axis. Alternatively, $\bar{\gamma}$ can be thought of as the azimuthal angle about the z axis [69]. In the two-thirds BF frame, the third Euler angle $\bar{\gamma} = 0$, which implies that the y axis lies in the XY plane. (b) The standard BF axes x', y', and z' are shown relative to the two-thirds BF axes x, y, and z, which are the same as in Fig. 7(a). The SF axes are omitted for clarity. The standard BF frame has the same z axis as the two-thirds BF frame ($z' = z$), but the third Euler angle $\bar{\gamma}$ is set equal to the azimuthal angle ϕ of **r** in the two-thirds BF frame such that the vector **r** lies in the $x'z'$ plane ($\mathbf{r}_{xy}$ is the projection of **r** onto the xy plane).

Another commonly used BF frame (the "standard" BF frame in the following or the "three-angle embedding" frame [80]) may be obtained from the two-thirds BF frame via an additional rotation about the z axis, which brings the diatomic molecule vector **r** to the $x'z'$ plane [80]. Figure 5(b) illustrates the orientation of the standard BF axes x', y', and z' relative to the two-thirds BF axes x, y, and z. The standard BF frame has the same z axis as the two-thirds BF frame ($z' = z$), but its x' and y' axes are rotated with respect to the two-thirds BF axes in the xy plane. The angle of rotation is the azimuthal angle ϕ of the diatomic molecule in the two-thirds BF frame [80], which is thereby identified with the third Euler angle ($\bar{\gamma} = \phi$).

By definition, the vector **r** always lies in the $x'z'$ plane, so only a single azimuthal angle θ is necessary to completely specify the orientation of the diatomic molecule in the standard BF frame. Accordingly, the basis functions in the standard BF frame can be written as [70]

$$\left(\frac{2J+1}{4\pi}\right)^{1/2} D_{M\Omega}^{J*}(\bar{\alpha}, \bar{\beta}, \phi) Y_{NK_N}(\theta, 0). \tag{A2}$$

The definitions (A1) and (A2) are equivalent because, as stated above, the third Euler angle $\bar{\gamma}$ used to define the standard BF frame is identical to the azimuthal angle ϕ of the diatomic molecule in the two-thirds BF frame. In this work, we choose to use the standard BF frame, which leads to simpler expressions for the matrix elements of the BF total angular momentum operator $\hat{J}$ [70,80].

APPENDIX B: VERIFICATION OF SCATTERING RESULTS

The BF theory of molecular collisions in the total angular momentum representation has been extensively tested [35] by comparison with the previous results obtained independently using the fully uncoupled SF representation of Volpi and Bohn [37] and Krems and Dalgarno [33]. To verify the correctness of the scattering cross sections calculated here for Rb + SrF, we have performed additional benchmark calculations using the independently developed codes SF2Sigma and extended MOLSCAT. SF2Sigma is a code developed in-house which uses the fully uncoupled SF basis [33,37] and extended MOLSCAT is a well-established package of programs for molecular scattering calculations [81] that has recently been extended [82] to handle molecular collisions in magnetic fields using the BF basis of Eq. (6).

For the purpose of comparison with SF calculations, we restrict our test calculations to small rotational basis sets ($N_{max} = 2$). This restriction is necessary because benchmark scattering calculations employing SF basis sets become computationally intractable for larger rotational basis sets with $N_{max} \geqslant 7$ [34,46], and hence cannot be used to obtain converged results for strongly anisotropic atom-molecule collision systems [46,55].

The total elastic and inelastic cross sections for Rb + SrF collisions computed here using the BF basis (6) are compared with the extended MOLSCAT and SF2Sigma results in Table II. All of the results are in excellent agreement with each other, thereby providing strong evidence for the validity of our quantum scattering approach and for the correctness of

TABLE II. Elastic and inelastic cross sections for ultracold Rb + SrF collisions computed using the BF code developed in the present work (first column), SF2Sigma (second column), and extended MOLSCAT (third column) at a magnetic field of 0.1 T. The collision energies are in units of cm^{-1} and the cross sections are in units of Å^2. The SF basis given by Eq. (10) of Ref. [33] included all the $|NM_N\rangle|lM_l\rangle$ states with $l \leqslant 7$ and $N \leqslant 2$ and the BF basis (6) included all the basis states with $J \leqslant 7$ and $N \leqslant 2$.

Collision energy	Present work	SF2Sigma	Extended MOLSCAT
Elastic cross sections			
10^{-5}	6.521×10^5	6.522×10^5	6.528×10^5
10^{-4}	1.143×10^5	1.142×10^5	1.142×10^5
10^{-3}	2.991×10^4	2.990×10^4	2.988×10^4
Inelastic cross sections			
10^{-5}	432.24	432.24	433.23
10^{-4}	3.080	3.080	3.084
10^{-3}	0.509	0.511	0.508

the Rb + SrF elastic and inelastic cross sections computed in this work.

APPENDIX C: BASIS SET CONVERGENCE

In this section, we examine the convergence properties of the Rb + SrF cross sections with respect to the basis set truncation parameters J_{max} and N_{max}, which determine the maximum quantum numbers of the total angular momentum J of the Rb-SrF collision complex and the rotational angular momentum N of SrF.

The convergence of the elastic (σ_{el}) and inelastic (σ_{inel}) cross sections for fully spin-polarized Rb-SrF collisions with respect to the value of N_{max} is illustrated in Fig. 6 for $B = 100$ G, $J_{max} = 1$, and $E_C = 10^{-6}$ cm^{-1}. The cross sections display rapid oscillations, which persist until $N_{max} \geqslant 110$, and we find that using $N_{max} = 125$ is nec-
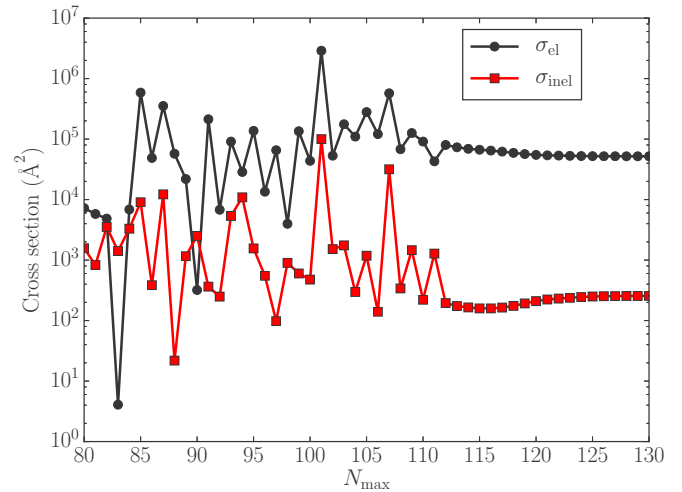

FIG. 6. Convergence of the elastic and inelastic cross sections with respect to the number of rotational states included in the basis set at the collision energy of 10^{-6} cm^{-1}. The magnetic field is 100 G and $J_{max} = 1$.
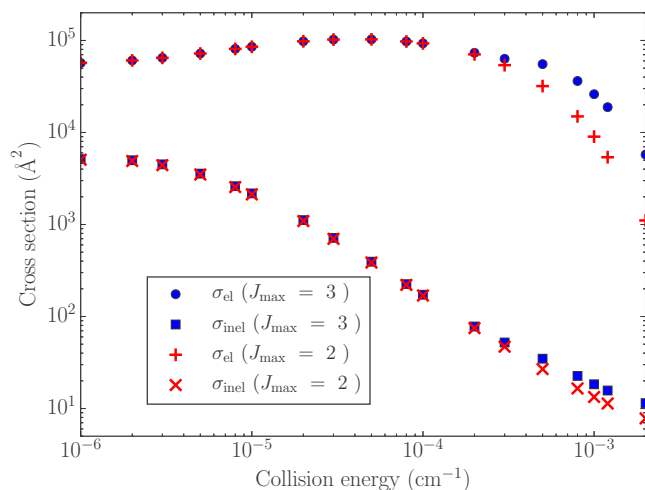
FIG. 7. Convergence of the elastic and inelastic cross sections with respect to the maximum total angular momentum value in the basis set: $J_{max} = 3$ (circles and squares) and $J_{max} = 2$ (pluses and crosses). The magnetic field is 100 G.

essary to produce the cross sections converged to within 2.5%.

To examine the convergence with respect to the maximum value of the total angular momentum J_{max}, we plot the elastic and inelastic cross sections as a function of collision energy in Fig. 7 for $J_{max} = 2$ and 3 at $B = 100$ G. Adequate convergence is achieved with $J_{max} = 2$ through the entire collision energy region. As discussed previously [33,34,37,47], indirect spin relaxation in the incoming s-wave channel must be accompanied by a change of the orbital angular momentum from $l = 0$ to $l = 2$. As a result, in order to properly describe the d-wave states in the outgoing collision channels, it is necessary to include at least four total angular momentum states ($J_{max} \geqslant 3$) in the basis set. On the other hand, the incoming p wave can make a transition to the outgoing p wave by changing m_l, the projection of l on the magnetic-field axis. Thus the s and p waves in the entrance and exit collision channels can be described by a smaller basis set with $J_{max} = 2$. To properly account for all of the partial waves in the entrance and exit collision channels, we choose to use $J_{max} = 3$ and $N_{max} = 125$ for the production calculations.

[1] L. D. Carr, D. DeMille, R. V. Krems, and J. Ye, Cold and ultracold molecules: science, technology and applications, New J. Phys. **11**, 055049 (2009).

[2] M. Lemeshko, R. V. Krems, J. M. Doyle, and S. Kais, Manipulation of molecules with electromagnetic fields, Mol. Phys. **111**, 1648 (2013).

[3] B. K. Stuhl, M. T. Hummon, and J. Ye, Cold state-selected molecular collisions and reactions, Annu. Rev. Phys. Chem. **65**, 501 (2014).

[4] R. V. Krems, Cold controlled chemistry, Phys. Chem. Chem. Phys. **10**, 4079 (2008).

[5] T. V. Tscherbul, G. Groenenboom, R. V. Krems, and A. Dalgarno, Dynamics of OH($^2\Pi$)-He collisions in combined electric and magnetic fields, Faraday Discuss. **142**, 127 (2009).

[6] T. V. Tscherbul and R. V. Krems, Controlling Electronic Spin Relaxation of Cold Molecules with Electric Fields, Phys. Rev. Lett. **97**, 083201 (2006).

[7] S. Ospelkaus, K.-K. Ni, D. Wang, M. H. G. de Miranda, B. Neyenhuis, G. Quéméner, P. S. Julienne, J. L. Bohn, D. S. Jin, and J. Ye, Quantum-state controlled chemical reaction of ultracold KRb molecules, Science **327**, 853 (2010).

[8] K.-K. Ni, S. Ospelkaus, D. Wang, G. Quéméner, B. Neyenhuis, M. H. G. de Miranda, J. L. Bohn, J. Ye, and D. S. Jin, Dipolar collisions of polar molecules in the quantum regime, Nature (London) **464**, 1324 (2010).

[9] M. H. G. de Miranda, A. Chotia, B. Neyenhuis, D. Wang, G. Quéméner, S. Ospelkaus, J. L. Bohn, J. Ye, and D. S. Jin, Controlling the quantum stereodynamics of ultracold bimolecular reactions, Nat. Phys. **7**, 502 (2011).

[10] B. K. Kendrick, J. Hazra, and N. Balakrishnan, The geometric phase controls ultracold chemistry, Nat. Commun. **6**, 7918 (2015).

[11] J. F. E. Croft and J. L. Bohn, Long-lived complexes and chaos in ultracold molecular collisions, Phys. Rev. A **89**, 012714 (2014).

[12] J. F. E. Croft, C. Makrides, M. Li, A. Petrov, B. K. Kendrick, N. Balakrishnan, and S. Kotochigova, Universality and chaoticity in ultracold K+KRb chemical reactions, Nat. Commun. **8**, 15897 (2017).

[13] T. V. Tscherbul and R. V. Krems, Tuning Bimolecular Chemical Reactions by Electric Fields, Phys. Rev. Lett. **115**, 023201 (2015).

[14] J. D. Weinstein, R. deCarvalho, T. Guillet, B. Friedrich, and J. M. Doyle, Magnetic trapping of calcium monohydride molecules at millikelvin temperatures, Nature (London) **395**, 148 (1998).

[15] W. C. Campbell, E. Tsikata, H.-I. Lu, L. D. van Buuren, and J. M. Doyle, Magnetic Trapping and Zeeman Relaxation of NH($^3\Sigma^-$), Phys. Rev. Lett. **98**, 213001 (2007).

[16] S. Y. T. van de Meerakker, P. H. M. Smeets, N. Vanhaecke, R. T. Jongma, and G. Meijer, Deceleration and Electrostatic Trapping of OH Radicals, Phys. Rev. Lett. **94**, 023004 (2005).

[17] N. Akerman, M. Karpov, Y. Segev, N. Bibelnik, J. Narevicius, and E. Narevicius, Trapping of Molecular Oxygen Together with Lithium Atoms, Phys. Rev. Lett. **119**, 073204 (2017).

[18] H.-I. Lu, I. Kozyryev, B. Hemmerling, J. Piskorski, and J. M. Doyle, Magnetic Trapping of Molecules via Optical Loading and Magnetic Slowing, Phys. Rev. Lett. **112**, 113006 (2014).

[19] Y. Liu, M. Vashishta, P. Djuricanin, S. Zhou, W. Zhong, T. Mittertreiner, D. Carty, and T. Momose, Magnetic Trapping of Cold Methyl Radicals, Phys. Rev. Lett. **118**, 093201 (2017).

[20] I. Kozyryev, L. Baum, K. Matsuda, B. L. Augenbraun, L. Anderegg, A. P. Sedlack, and J. M. Doyle, Sisyphus Laser Cooling of a Polyatomic Molecule, Phys. Rev. Lett. **118**, 173201 (2017).

[21] J. F. Barry, D. J. McCarron, E. B. Norrgard, M. H. Steinecker, and D. DeMille, Magneto-optical trapping of a diatomic molecule, Nature (London) **512**, 286 (2014).

[22] J. Barry, Laser cooling and slowing of a diatomic molecule, Ph.D. thesis, Yale University, 2013.

[23] E. B. Norrgard, D. J. McCarron, M. H. Steinecker, M. R. Tarbutt, and D. DeMille, Submillikelvin Dipolar Molecules in a Radio-Frequency Magneto-Optical Trap, Phys. Rev. Lett. **116**, 063004 (2016).

[24] M. T. Hummon, M. Yeo, B. K. Stuhl, A. L. Collopy, Y. Xia, and J. Ye, 2D Magneto-Optical Trapping of Diatomic Molecules, Phys. Rev. Lett. **110**, 143001 (2013).

[25] S. Truppe, H. J. Williams, M. Hambach, L. Caldwell, N. J. Fitch, E. A. Hinds, B. E. Sauer, and M. R. Tarbutt, Molecules cooled below the Doppler limit, Nat. Phys. **13**, 1173 (2017).

[26] H. J. Williams, L. Caldwell, N. J. Fitch, S. Truppe, J. Rodewald, E. A. Hinds, B. E. Sauer, and M. R. Tarbutt, Magnetic Trapping and Coherent Control of Laser-Cooled Molecules, Phys. Rev. Lett. **120**, 163201 (2018).

[27] D. J. McCarron, M. H. Steinecker, Y. Zhu, and D. DeMille, Magnetic Trapping of an Ultracold Gas of Polar Molecules, Phys. Rev. Lett. **121**, 013202 (2018).

[28] L. Anderegg, B. L. Augenbraun, Y. Bao, S. Burchesky, L. W. Cheuk, W. Ketterle, and J. M. Doyle, Laser cooling of optically trapped molecules, Nat. Phys. **14**, 890 (2018).

[29] C. Chin, R. Grimm, P. Julienne, and E. Tiesinga, Feshbach resonances in ultracold gases, Rev. Mod. Phys. **82**, 1225 (2010).

[30] M. Lara, J. L. Bohn, D. Potter, P. Soldan, and J. M. Hutson, Ultracold Rb-OH Collisions and Prospects for Sympathetic Cooling, Phys. Rev. Lett. **97**, 183201 (2006).

[31] G. Modugno, G. Ferrari, G. Roati, R. J. Brecha, A. Simoni, and M. Inguscio, Bose-Einstein condensation of potassium atoms by sympathetic cooling, Science **294**, 1320 (2001).

[32] S. Aubin, S. Myrskog, M. H. T. Extavour, L. J. Leblanc, D. Mckay, A. Stummer, and J. H. Thywissen, Rapid sympathetic cooling to Fermi degeneracy on a chip, Nat. Phys. **2**, 384 (2006).

[33] R. V. Krems and A. Dalgarno, Quantum-mechanical theory of atom-molecule and molecular collisions in a magnetic field: Spin depolarization, J. Chem. Phys. **120**, 2296 (2004).

[34] T. V. Tscherbul, Effects of external magnetic fields on cold molecular collisions, in *Low Energy and Low Temperature Molecular Scattering*, edited by A. Osterwalder and O. Dulieu (Royal Society of Chemistry, London, 2017).

[35] T. V. Tscherbul and A. Dalgarno, Quantum theory of molecular collisions in a magnetic field: Efficient calculations based on the total angular momentum representation, J. Chem. Phys. **133**, 184104 (2010).

[36] J. Lim, M. D. Frye, J. M. Hutson, and M. R. Tarbutt, Modeling sympathetic cooling of molecules by ultracold atoms, Phys. Rev. A **92**, 053419 (2015).

[37] A. Volpi and J. L. Bohn, Magnetic-field effects in ultracold molecular collisions, Phys. Rev. A **65**, 052712 (2002).

[38] W. C. Campbell, T. V. Tscherbul, H.-I. Lu, E. Tsikata, R. V. Krems, and J. M. Doyle, Mechanism of Collisional Spin Relaxation in $^3\Sigma$ Molecules, Phys. Rev. Lett. **102**, 013003 (2009).

[39] E. A. Cornell and C. E. Wieman, Nobel lecture: Bose-Einstein condensation in a dilute gas, the first 70 years and some recent experiments, Rev. Mod. Phys. **74**, 875 (2002).

[40] W. Ketterle, Nobel lecture: When atoms behave as waves: Bose-Einstein condensation and the atom laser, Rev. Mod. Phys. **74**, 1131 (2002).

[41] W. Ketterle and N. J. Van Druten, Evaporative cooling of trapped atoms, Adv. At., Mol., Opt. Phys. **37**, 181 (1996).

[42] A. O. G. Wallis and J. M. Hutson, Production of Ultracold NH Molecules by Sympathetic Cooling with Mg, Phys. Rev. Lett. **103**, 183201 (2009).

[43] M. T. Hummon, T. V. Tscherbul, J. Kłos, H.-I. Lu, E. Tsikata, W. C. Campbell, A. Dalgarno, and J. M. Doyle, Cold N + NH Collisions in a Magnetic Trap, Phys. Rev. Lett. **106**, 053201 (2011).

[44] P. Żuchowski and J. M. Hutson, Cold collisions of N atoms and NH molecules in magnetic fields, Phys. Chem. Chem. Phys. **13**, 3669 (2011).

[45] M. L. González-Martínez and J. M. Hutson, Ultracold Hydrogen Atoms: A Versatile Coolant to Produce Ultracold Molecules, Phys. Rev. Lett. **111**, 203004 (2013).

[46] T. V. Tscherbul, J. Kłos, and A. A. Buchachenko, Ultracold spin-polarized mixtures of $^2\Sigma$ molecules with S-state atoms: Collisional stability and implications for sympathetic cooling, Phys. Rev. A **84**, 040701(R) (2011).

[47] M. Morita, J. Kłos, A. A. Buchachenko, and T. V. Tscherbul, Cold collisions of heavy $^2\Sigma$ molecules with alkali-metal atoms in a magnetic field: *Ab initio* analysis and prospects for sympathetic cooling of SrOH($^2\Sigma$) by Li(^{2}S), Phys. Rev. A **95**, 063421 (2017).

[48] R. V. Krems, A. Dalgarno, N. Balakrishnan and G. C. Groenenboom, Spin-flipping transitions in $^2\Sigma$ molecules induced by collisions with structureless atoms, Phys. Rev. A **67**, 060703 (2003).

[49] V. Singh, K. S. Hardman, N. Tariq, M.-J. Lu, A. Ellis, M. J. Morrison, and J. D. Weinstein, Chemical Reactions of Atomic Lithium and Molecular Calcium Monohydride at 1 K, Phys. Rev. Lett. **108**, 203201 (2012).

[50] M. B. Kosicki, D. Kędziera, and P. S. Żuchowski, Ab initio study of chemical reactions of cold SrF and CaF molecules with alkali-metal and alkaline-earth-metal atoms: The implications for sympathetic cooling, J. Phys. Chem. A **121**, 4152 (2017).

[51] E. R. Meyer and J. L. Bohn, Chemical pathways in ultracold reactions of SrF molecules, Phys. Rev. A **83**, 032714 (2011).

[52] E. Abrahamsson, T. V. Tscherbul, and R. V. Krems, Inelastic collisions of cold polar molecules in nonparallel electric and magnetic fields, J. Chem. Phys. **127**, 044302 (2007).

[53] M. Warehime and J. Kłos, Nonadiabatic collisions of CaH with Li: Importance of spin-orbit-induced spin relaxation in spin-polarized sympathetic cooling of CaH, Phys. Rev. A **92**, 032703 (2015).

[54] L. M. C. Janssen, A. van der Avoird, and G. C. Groenenboom, Quantum Reactive Scattering of Ultracold NH($X^3\Sigma^-$) Radicals in a Magnetic Trap, Phys. Rev. Lett. **110**, 063201 (2013).

[55] Yu. V. Suleimanov and T. V. Tscherbul, Cold NH-NH collisions in a magnetic field: Basis set convergence versus sensitivity to the interaction potential, J. Phys. B **49**, 204002 (2016).

[56] C. Hampel, K. Peterson, and H.-J. Werner, A comparison of the efficiency and accuracy of the quadratic configuration interaction (QCISD), coupled cluster (CCSD), and Brueckner

coupled cluster (BCCD) methods, Chem. Phys. Lett. **190**, 1 (1992).

[57] M. J. O. Deegan and P. J. Knowles, Perturbative corrections to account for triple excitations in closed and open shell coupled cluster theories, Chem. Phys. Lett. **227**, 321 (1994).

[58] H.-J. Werner, P. J. Knowles, G. Knizia, F. R. Manby, M. Schütz, P. Celani, W. Györffy, D. Kats, T. Korona, R. Lindh *et al.*, *MOLPRO*, version 2015.1: A package of ab initio programs, see http://www.molpro.net.

[59] I. S. Lim, P. Schwerdtfeger, B. Metz, and H. Stoll, All-electron and relativistic pseudopotential studies for the group 1 element polarizabilities from K to element 119, J. Chem. Phys. **122**, 104103 (2005).

[60] I. S. Lim, H. Stoll, and P. Schwerdtfeger, Relativistic small-core energy-consistent pseudopotentials for the alkaline-earth elements from Ca to Ra, J. Chem. Phys. **124**, 034107 (2006).

[61] S. F. Boys and F. Bernardi, The calculation of small molecular interactions by the differences of separate total energies. Some procedures with reduced errors, Mol. Phys. **19**, 553 (1970).

[62] K. P. Huber and G. Herzberg, *Molecular Spectra and Molecular Structure, IV. Constants of Diatomic Molecules* (Van Nostrand Reinhold, New York, 1979).

[63] T. S. Ho and H. Rabitz, A general method for constructing multidimensional molecular potential energy surfaces from *ab initio* calculations, J. Chem. Phys. **104**, 2584 (1996).

[64] T. J. Lee and P. R. Taylor, A diagnostic for determining the quality of single-reference electron correlation methods, Int. J. Quantum Chem., Quantum Chem. Symp. **S23**, 199 (1989).

[65] L. M. C. Janssen, G. C. Groenenboom, A. Van Der Avoird, P. S. Zuchowski, and R. Podeszwa, Ab initio potential energy surfaces for $NH(^3\Sigma^-)$-$NH(^3\Sigma^-)$ with analytical long range, J. Chem. Phys. **131**, 224314 (2009).

[66] M. Karplus and R. N. Porter, in *Atoms and Molecules: An Introduction for Students of Physical Chemistry* (Benjamin, New York, 1970), p. 24.

[67] T. V. Tscherbul, J. Kłos, A. Dalgarno, B. Zygelman, Z. Pavlovic, M. T. Hummon, H.-I. Lu, E. Tsikata, and J. M. Doyle, Collisional properties of cold spin-polarized nitrogen gas: Theory, experiment, and prospects as a sympathetic coolant for trapped atoms and molecules, Phys. Rev. A **82**, 042718 (2010).

[68] Yu. V. Suleimanov, T. V. Tscherbul, and R. V. Krems, Efficient method for quantum calculations of molecule-molecule scattering properties in a magnetic field, J. Chem. Phys. **137**, 024103 (2012).

[69] R. N. Zare, *Angular Momentum* (Wiley, New York, 1988).

[70] J. M. Hutson, Adv. Mol. Vibr. Coll. Dyn. A **1**, 1 (1990).

[71] A. van der Avoird, P. E. S. Wormer, and R. Moszynski, From intermolecular potential to the spectra of van der Waals molecules and vice versa, Chem. Rev. **94**, 1931 (1994).

[72] G. G. Balint-Kurti, The theory of rotationally inelastic molecular collisions, in *International Review of Science*, edited by A. D. Buckingham and C. A. Coulson (Butterworths, London, 1975), Ser. II, Vol. 1, p. 286.

[73] J. Tennyson and B. T. Sutcliffe, The ab initio calculation of the vibrational-rotational spectrum of triatomic systems in the close-coupling approach, with KCN and H_2Ne as examples, J. Chem. Phys. **77**, 4061 (1982).

[74] D. E. Manolopoulos, An improved log-derivative method for inelastic scattering, J. Chem. Phys. **85**, 6425 (1986).

[75] M. H. Alexander and D. E. Manolopoulos, A stable linear reference potential algorithm for solution of the quantum close-coupled equations in molecular scattering theory, J. Chem. Phys. **86**, 2044 (1987).

[76] B. R. Johnson, The multichannel log-derivative method for scattering calculations, J. Comput. Phys. **13**, 445 (1973).

[77] J. M. Hutson, M. Beyene, and M. L. González-Martínez, Dramatic Reductions in Inelastic Cross Sections for Ultracold Collisions near Feshbach Resonances, Phys. Rev. Lett. **103**, 163201 (2009).

[78] L. M. C. Janssen, P. S. Żuchowski, A. van der Avoird, G. C. Groenenboom, and J. M. Hutson, Cold and ultracold NH-NH collisions in magnetic fields, Phys. Rev. A **83**, 022713 (2011).

[79] L. M. C. Janssen, A. van der Avoird, and G. C. Groenenboom, On the role of the magnetic dipolar interaction in cold and ultracold collisions: Numerical and analytical results for $NH(^3\Sigma)$ + $NH(^3\Sigma)$, Eur. Phys. J. D **65**, 177 (2011).

[80] G. Brocks, A. van der Avoird, B. T. Sutcliffe, and J. Tennyson, Quantum dynamics of non-rigid systems comprising two polyatomic fragments, Mol. Phys. **50**, 1025 (1983).

[81] J. M. Hutson and S. Green, MOLSCAT computer code, version 14, distributed by Collaborative Computational Project No. 6 of the Engineering and Physical Sciences Research Council, UK, 1994.

[82] M. Frye, M. Morita, C. L. Vaillant, D. Green, and J. M. Hutson, Approach to chaos in ultracold atomic and molecular physics: Statistics of near-threshold bound states for Li+CaH and Li+CaF, Phys. Rev. A **93**, 052713 (2016).